Performance Analysis of a Solar-assisted OTEC Cycle for Power Generation and Fishery Cold Storage Refrigeration

Han Yuan[1, 2], Peilin Zhou[2] and Ning Mei[1*]

1. College of Engineering, Ocean University of China, 238 Songling Road, Laoshan district, Qingdao 266100, China

2. Department of Naval Architecture and Marine Engineering, University of Strathclyde, Glasgow G4 0LZ, United Kingdom

*. Corresponding author,

Phone/Fax: +86-532-66781105,

E-mail: nmei@ouc.edu.cn,

Address: 238 Songling Road, Laoshan district, Qingdao 266100, China

Abstract

The cold storage in fishery industry is in great demand in tropical coastal regions. This research proposes an ocean thermal energy conversion (OTEC) based solar-assisted combined power and refrigeration cycle, which can be used for both electricity generation and fishery cold storage application. In this proposed combined cycle, the ammonia/water is selected as the working fluid and the warm/cold seawater is utilized as the heating/cooling source. A two-stage ejector system is

Accepted author manuscript of the following research article: Yuan, H., Zhou, P., & Mei, N. (2015). Performance analysis of a solar-assisted OTEC cycle for power generation and fishery cold storage refrigeration. Applied Thermal Engineering, 90, 809-819. DOI: 10.1016/j.applthermaleng.2015.07.072

introduced, the turbine is used to produce power and the evaporator is used to produce refrigeration output. Besides, a flat-plate solar collector is utilized to increase the heating source temperature. To evaluate the performance of the proposed cycle, a mathematical model is developed and a simulation program is developed; the performance comparison between it and a previous two-stage ejector OTEC cycle is made, which shows this solar-assisted cycle has a slightly lower power-production efficiency of 2.27% but a much higher comprehensive-production efficiency of 7.89% under the given working condition. Furthermore, parametric analysis is performed to guide the theoretical performance of this combined cycle. The results show that the generator pressure, solar collector outlet temperature and rich solution concentration all affect the cycle performance; the entrainment ratio of the first-stage ejector is greatly affected by the rich solution concentration.

Keywords: OTEC; combined power and refrigeration cycle; solar energy; ammonia/water; ejector

Nomenclature

Symbols

A	area, m^2
I	solar radiation intensity, W m^{-2}
k	solar collector global losses factor
T	temperature, K
c_P	seawater specific heat, kJ $kg^{-1}K^{-1}$
U	heat transfer coefficient, kW m^2 K
Q	input, kJ
W	turbine output, kJ

m	mass flow rate, kg s^{-1}
h	specific enthalpy, kJ kg^{-1}
P	pressure, MPa
X_r	rich solution concentration, kg kg^{-1}
X_w	weak solution concentration, kg kg^{-1}
g	gravitational acceleration, m s^{-2}
Greek Symbols	
α	solar collector absorption surface factor
β	expansion ratio
τ	solar collector transmission factor
Δ	temperature difference
μ	entrainment ratio
v	specific volume, m^3 kg^{-1}
η	efficiency, %
Subscripts	
I, II	apparatus number
i=1, 2, 3……	state points
ave	solar collector absorption surface average temperature
a	environment average temperature
ws	warm seawater
SC	solar collector
lm	logarithmic mean

G	generator
Ab	absorber
E	evaporator
T	turbine
SP	solution pump
SWP	seawater pump
WP	warm seawater pump
CP	cold seawater pump
pf	primary flow
sf	secondary flow
d	diffuser
n	nozzle
m	mixing chamber
s	solution mixture
s'	isentropic process
n1	nozzle inlet
n2	nozzle outlet
net	net work
eff	effective
e	exergy
ref	refrigeration
Acronyms	
OTEC	ocean thermal energy conversion

1. Introduction

The development of cold storage for fishery industry in certain tropical coastal regions is less than satisfactory. According to data of Indonesia Ministry of Marine Affairs and Fisheries, this island nation ranks the tenth highest fishery producer in the world, but only 2 out of total 6 of its ocean fishing ports possess cold storage facilities. Moreover, only 4 out of total 14 national fishery ports own cold storage facilities [1]. The lack of cold storage facilities has greatly restricted the development of its fishery industry. Under this circumstance, programs and technologies that can encourage the development of cold storage in this region is in extremely great demand.

It is interesting to note that these tropical regions are also particularly suitable for applying the ocean thermal energy conversion (OTEC) technology. OTEC technology provides a method of exploiting the solar energy absorbed in the upper layer of the ocean. In an OTEC system, a thermodynamic cycle, driven by the temperature difference between the top warm seawater (26-30^{o}C) and the deep cold seawater (4-6^{o}C), is used to produce power. Great efforts were made in the development of OTEC and a series of pilot plants were built [2-6] . As is discussed in Ref.[7], the mean annual temperature difference between depth of 20m and 1000m along the west coast of Pacific Ocean remains at the highest value of 24-26^{o}C throughout the world, which permits this region an optimum place for OTEC development. If an OTEC technology based thermodynamic cycle can be applied for both power and refrigeration production purpose, the fishery cold-storage problem in these tropical costal region can be solved.

As is known, the combined power and refrigeration cycle is widely applied for power and refrigeration production, but this kind of thermodynamic cycle is deemed to be not applicable in the OTEC application. This is because the warm seawater temperature is too low to drive a combined cycle. However, the solar-assisted OTEC cycle, which has attracted researchers' attention in recent

years [8-12], shows a potential of solving the heating source problem. By introducing a solar collector in the OTEC cycle, the warm seawater temperature can be dramatically increased (normally to higher than 80^{o}C).

Also, the performance of the OTEC cycle needs to be concerned. Actually, the development of the OTEC technology has been greatly restricted due to its low level of thermal efficiency. With the relatively small temperature difference between the heating and cooling source, the Carnot cycle efficiency for an OTEC system is limited at 8% [13]. Till now, massive researches have been made to improve the thermal efficiency for OTEC cycle. Among different kinds of working fluids, the ammonia/water, a binary solution, was proved to be more effective for an OTEC system [14, 15]. Compared with an organic working fluid, the ammonia/water evaporates or condenses over a range of temperature, which leads to a lower temperature difference in the evaporation or condensation process, and in this way an ammonia/water based cycle can reduce the heat transfer related irreversibility occurs in the evaporator and condenser [16-18]. The “Kalina cycle” was the first proposed ammonia/water based OTEC power cycle, which was reported to have better thermal efficiency than the conventional Rankine cycle at the same temperature difference [19]. Uehara modified the Kalina cycle and proposed a better performed “Uehara cycle” [20]. Further, Yuan proposed an ammonia/water based two-stage ejector OTEC cycle [21]. By employing an additional ejector sub-cycle, the proposed cycle can be driven with a lower temperature difference, resulting in a better thermodynamic performance.

In this study, we propose a OTEC based solar-assisted combined power and refrigeration cycle. A two-stage ejector system is introduced in this combined cycle; the ammonia-water is used as the working fluid. By utilizing not only ocean thermal energy but also solar energy, this combined cycle can produce both power output for electricity generation purpose, and refrigeration outputs for fishery cold storage, simultaneously.

This study will establish the mathematical model for the proposed combined cycle. Also, its performance will be compared with a previous two-stage ejector OTEC cycle. Further, parametric analysis will be conducted to examine the effects of thermodynamic parameters on the performance of this combined cycle.

2. System description

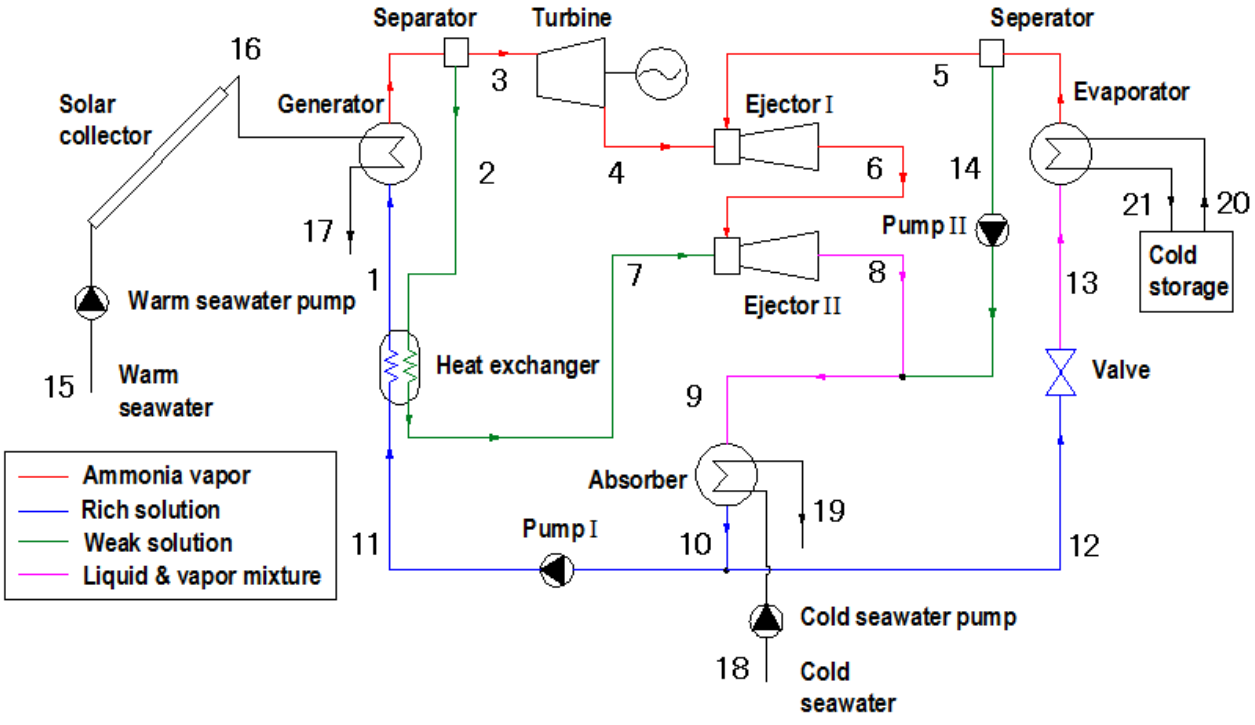

Fig.1 Schematic of the solar-assisted combined power and ejector refrigeration cycle

Fig. 1 shows the schematic of the combined cycle. The proposed cycle consists of the following main components:

- A generator

- An evaporator
- An absorber
- A flat-plate solar collector
- A heat exchanger
- A turbine
- Two separators
- Two ejectors
- Two solution pumps
- A throttle valve

In this combined cycle, the turbine is used to produce power and the evaporator is introduced to produce refrigeration output, the ammonia/water is selected as the working fluid and the warm/cold seawater is used as the heating/cooling source.

The warm seawater is pumped into the solar collector to absorb solar energy. The relatively higher temperature seawater is then used to evaporate the rich ammonia-water solution restored in the generator. The mixture of both ammonia and water vapor is generated in this process and then separated in the separator. The ammonia vapor (at state point 3) drives the turbine to produce power, before flows into the ejector I as the primary fluid (at state point 4). Meanwhile, the ammonia vapor (at state point 5) evaporated in the evaporator is separated and sucked into the ejector I as the second fluid. These two ammonia vapors are first mixed in the ejector I, and then sucked into the ejector II as the second fluid. Simultaneously, the relatively high pressure weak solution (at state point 2) is

cooled in the heat exchanger and flows into the ejector II as the primary fluid. Further, the liquid and vapor mixture (at state point 8), along with the separated weak solution (at state point 14), flows into the absorber to produce the rich solution (at state point 10). The cold seawater is used to take away heat generated in the absorption process. Finally, the rich solution at a relatively low temperature and pressure divides into two branches: one is pumped into the generator after heated in the heat exchanger; the other enters the evaporator after passing through the throttle valve. The refrigeration is produced in the evaporation and the supplied to the cold storage through heating exchange.

3. Cycle modeling

3.1. Basic assumptions

The following assumptions were used in the cycle modelling:

- Each components of this combined cycle is in steady state.
- The pressure drop and heat losses in the cycle are neglected.
- The fluid expansion in the throttling valve is considered as isenthalpic.
- The ammonia-water solution/vapour at the outlet of both absorber and separators are saturated.
- The efficiency of the pumps and turbine are 85%.

3.2. Mathematical model

The mathematical model for this combined cycle was established on the basis of the first law of

thermodynamics, and energy analysis was conducted to evaluate the theoretical performance of this combined cycle.

The heat rate absorbed by the flat-plate solar collector is defined as follows (Hottel- Whillier-Bliss equation [22]):

$$Q_{SC} = A_{SC} \cdot I \cdot \eta_{SC} \quad (1)$$

Where A_{SC} is the solar collector effective area, I is the intensity of solar radiation. The solar collector thermal efficiency η_{SC} is defined as:

$$\eta_{SC} = \alpha\tau - k(T_{ave} - T_a)/I \quad (2)$$

Where the absorption surface factor α represents the percentage of the solar radiation being absorbed, the transmission factor τ estimates the heat losses of the solar radiation penetrating the transparent material. k is the global losses factor, varies from 1 to 30 W/m^2 K. $T_{ave}=(T_{15}+T_{16})/2$ is the average temperature of the solar collector absorption surface and T_a is the average temperature of the environment.

The solar collector heat input can also be defined as:

$$Q_{SC} = c_P m_{WS}(T_{16} - T_{15}) \quad (3)$$

Where c_P is the specific heat of seawater, m_{WS} is the mass flow rate of the warm seawater through the solar collector; T_{15} and T_{16} are the seawater temperature in both the inlet and outlet of the solar collector.

The heat conduction of the generator is:

$$Q_G = U_G A_G \Delta T_{lm,G} \quad (4)$$

Where U_G is the heat transfer coefficient, A_G is the cross-section area normal to the direction of the heat transfer, $\Delta T_{lm,G}$ is the logarithmic mean temperature difference of the generator expressed as:

$$\Delta T_{lm,G} = \frac{(T_{16} - T_2) - (T_{17} - T_1)}{\ln((T_{16} - T_2)/(T_{17} - T_1))} \quad (5)$$

And the heat conduction of the absorber is:

$$Q_{Ab} = U_{Ab} A_{Ab} \Delta T_{lm,Ab} \quad (6)$$

Where the logarithmic mean temperature difference of the absorber is:

$$\Delta T_{lm,Ab} = \frac{(T_9 - T_{19}) - (T_{10} - T_{18})}{\ln((T_9 - T_{19})/(T_{10} - T_{18}))} \quad (7)$$

The heat conduction of the evaporator is:

$$Q_E = U_E A_E \Delta T_{lm,E} \quad (8)$$

Where the logarithmic mean temperature difference of the evaporator is defined at 5K, for the temperature at state point 20 is an uncertain value, depending on the temperature of the cold storage inlet.

The mass balance equations in the cycle are given as follows:

$$\Delta_{\text{out}}^{\text{in}} \sum m_i = 0 \quad (9)$$

$$\Delta_{\text{out}}^{\text{in}} \sum X_i \cdot m_i = 0 \quad (10)$$

For the ejector, an one-dimensional flow model, which was first introduced by Keenan [23] and then developed by Huang [24] and Dai [25], is introduced to carry out the ejector's calculation.

The enthalpy balance equations for the ejectors [26] are given as follows:

$$(1+\mu_{\mathrm{I}})h_6 = \mu_{\mathrm{I}} h_5 + h_4 \tag{11}$$

$$(1+\mu_{\mathrm{II}})h_8 = \mu_{\mathrm{II}} h_6 + h_7 \tag{12}$$

$$\mu_{\mathrm{I}} = m_5 / m_4 \tag{13}$$

$$\mu_{\mathrm{II}} = m_6 / m_7 \tag{14}$$

Each ejector consists of three sections: the nozzle section, the mixing section and the diffuser section [25] .

For the nozzle section:

$$m_{\mathrm{pf}} h_{\mathrm{pf,n2}} + \frac{m_{\mathrm{pf}} u_{\mathrm{pf,n2}}^2}{2} = m_{\mathrm{pf}} h_{\mathrm{pf,n1}} + \frac{m_{\mathrm{pf}} u_{\mathrm{pf,n1}}^2}{2} \tag{15}$$

For the mixing section:

$$m_{\mathrm{pf}} h_{\mathrm{pf,n2}} + m_{\mathrm{pf}} u_{\mathrm{pf,n2}}^2 = (m_{\mathrm{pf}} + m_{\mathrm{sf}}) u_{\mathrm{mf,m,s}} \tag{16}$$

For the diffuser section:

$$\frac{1}{2}(u_{\mathrm{mf,m}}^2 - u_{\mathrm{mf,d,s'}}^2) = h_{\mathrm{mf,d,s'}} - h_{\mathrm{mf,m}} \tag{17}$$

The entrainment ratio of the ejectors can also be derived as:

$$\mu = \sqrt{\eta_{\mathrm{n}} \eta_{\mathrm{m}} \eta_{\mathrm{d}} (h_{\mathrm{pf,n1}} - h_{\mathrm{pf,n2,s'}}) / (h_{\mathrm{mf,d,s'}} - h_{\mathrm{mf,m}})} - 1 \tag{18}$$

Where, η_n is the nozzle efficiency, η_m is the mixing efficiency, η_d is the diffuser efficiency.

More detailed formulations for the ejector are described in Ref. [25]. The energy balance equations for each component are given as follows:

For the generator:

$$Q_G = m_3 h_3 + m_2 h_2 - m_1 h_1 \tag{19}$$

For the evaporator:

$$Q_E = m_5 h_5 + m_{14} h_{14} - m_{13} h_{13} \tag{20}$$

For the turbine:

$$W_T = \eta_T m(h_3 - h_4) \tag{21}$$

$$\beta = P_3 / P_4 \tag{22}$$

Where η_T is the turbine isentropic efficiency, which is greatly influenced by factors of such as working fluid property, operation pressure and temperature. As these factors vary in different thermodynamic cycles, the turbine efficiency varies a lot. In order to obtain a reliable turbine efficiency value, two parameters are investigated in this section: the turbine volumetric flow ratio (VFR), which reflects the compressibility effect through the expansion; the turbine size parameter (SP), which reflects the actual turbine size in detailed design [27, 28]. These two parameters are defined as:

$$VFR = \rho_1 / \rho_2 \tag{23}$$

$$SP = V_2^{1/2} / (h_1 - h_2)^{1/4} \tag{24}$$

Where ρ_1 and ρ_2 are the vapour density at turbine inlet and outlet, respectively; V_2 is the

volumetric flow at turbine outlet; h_1 and h_2 are the specific enthalpy of working fluid at turbine inlet and outlet, respectively.

For the absorber:

$$Q_{Ab} = m_9(h_9 - h_{10}) \tag{25}$$

For the heat exchanger:

$$m_2(h_2 - h_7) = m_1(h_{11} - h_1) \tag{26}$$

For the solution pumps:

$$W_{PI} = (P_{11} - P_{10})v_{10}m_{10} / \eta_{SP} \tag{27}$$

$$W_{PII} = (P_9 - P_{14})v_{14}m_{14} / \eta_{SP} \tag{28}$$

For the seawater pumps:

$$W_{WP} = m_{WP}\Delta H_{WP} g / \eta_{SWP} \tag{29}$$

$$W_{CP} = m_{CP}\Delta H_{CP} g / \eta_{SWP} \tag{30}$$

Where ΔH_{WP}, ΔH_{CP} are pump head difference of warm and cold seawater, which are obtained from the previous work [20].

The thermal efficiency is commonly used to evaluate a thermodynamic cycle performance, which is defined as the ratio of cycle output and to heat input. But this definition may cause some confusion when it is applied to a combined cycle. Without accounting for the quality of the refrigeration output, the total thermal efficiency would be overestimated [29].

To avoid this overestimation, two kinds of efficiency: the power efficiency and the effective efficiency are defined. The definition of the power efficiency is shown in Eq. (29). This efficiency expression represents the power generation capacity of the combined cycle.

The effective efficiency (Eq. (29)) can evaluate the quality difference between the power and refrigeration outputs [29]. Where, COP_{eff} is the practical efficiency of the refrigeration capacity Q_e. E_e represents the exergy associated with the refrigeration output. From another point of view, it can be considered as the available energy of the refrigeration output. η_{ref} is the second law efficiency for the combined cycle.

Power efficiency:

$$\eta = W_{net} / Q_{SC} \tag{31}$$

$$W_{net} = W_T - W_{PI} - W_{PII} - W_{WP} - W_{CP} \tag{32}$$

Effective efficiency:

$$\eta_{eff} = \frac{W_{net} + (Q_e / COP_{eff})}{Q_{SC}} = \frac{W_{net} + (E_e / \eta_{ref})}{Q_{SC}} \tag{33}$$

$$E_e = m[(h_{cool,in} - h_{cool,out}) - T_0(s_{cool,in} - s_{cool,out})] \tag{34}$$

$$\eta_{ref} = \frac{W_{net}}{Q_G(1 - T_a / T_{16})} \tag{35}$$

4. System simulation strategy and validation

4.1. Initial condition for analysis

241 An initial working condition for this combined cycle was specified. The warm seawater
242 temperature is assumed to be 299K (26ºC) and the cold seawater temperature is 277K (4ºC); the initial
243 ammonia/water rich solution concentration is 0.7 kg kg^{-1}. All the details of this initial working
244 condition are listed in Table 1. It should be noted that the turbine isentropic efficiency is fixed at 85%
245 in this simulation. This value is based on the investigation of the turbine VFR and SP for the combined
246 cycle, which is discussed in section 5.

247 **Table 1**

248 Initial working condition

Turbine isentropic efficiency, η_T	0.85
Seawater pump isentropic efficiency, η_{SWP}	0.80
Solution pump isentropic efficiency, η_{SP}	0.75
Ambient temperature, T_a (K)	298
Solar radiation intensity, I (W m^{-2})	500 [8]
Solar collector absorption surface factor, α	0.90
Solar collector transmission factor, τ	0.85
Solar collector global losses factor, k	1.70
Solar collector effective area, A_{SC} (m^2)	8,000
Seawater specific heat capacity, c_P (kJ $kg^{-1}K^{-1}$)	4.025
Seawater density, ρ (kg m^3)	1025
Warm seawater mass flow rate, m_{WS} (kg s^{-1})	26
Cold seawater mass flow rate, m_{CS} (kg s^{-1})	26
Warm seawater temperature, T_{15} (K)	26
Cold seawater temperature, T_{18} (K)	4

Pump head difference of warm seawater, ΔH_{WP} (m)	2.5
Pump head difference of cold seawater, ΔH_{CP} (m)	5.6
Generator heat transfer coefficient, U_G (kW m^2 K)	4.0
Absorber heat transfer coefficient, U_{Ab} (kW m^2 K)	3.5
Evaporator heat transfer coefficient, U_E (kW m^2 K)	4.0
Generation pressure, P_G (MPa)	1.0
Rich solution concentration, X_r (kg kg^{-1})	0.7
Turbine expansion ratio, β	1.5
Nozzle efficiency, η_n (%)	90 [25]
Mixing efficiency, η_m (%)	85
Diffuser efficiency, η_d (%)	85

4.2. Solution procedure

Based on the above model a simulation program was developed. Fig. 2 shows the calculation flow chart. In this program, the thermodynamic properties of ammonia-water and ammonia-vapour were determined by the Sulze Equation [30].

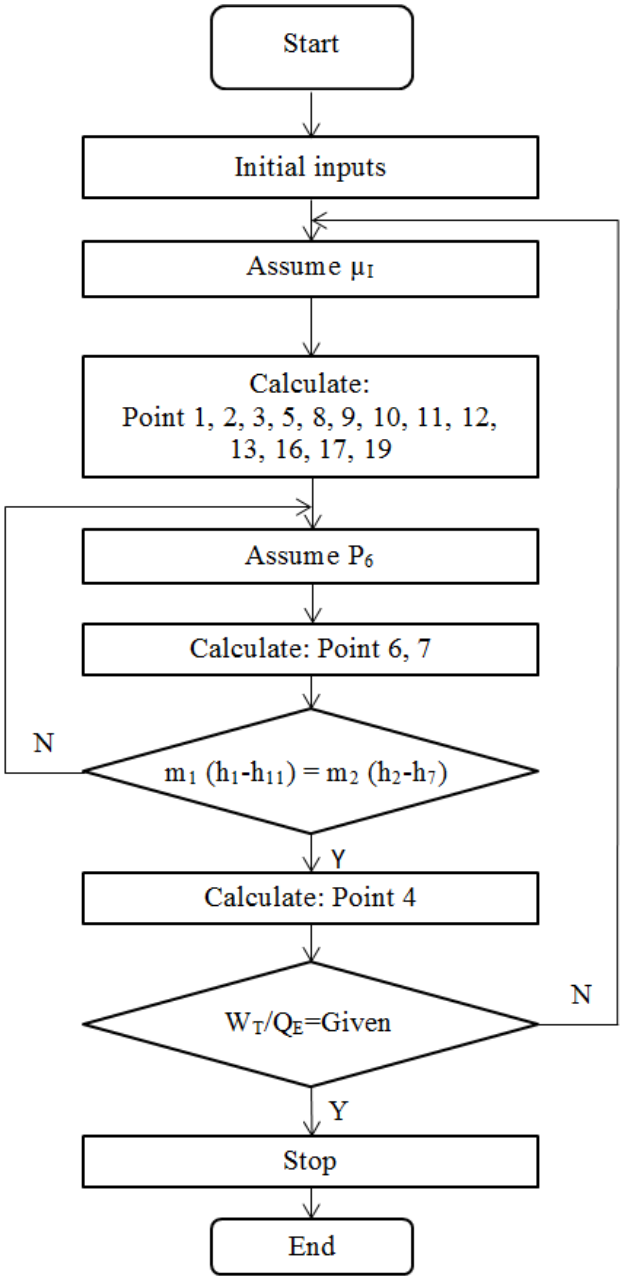

Fig.2 Flow chart of the combined cycle

4.3. Rationality validation of simulation

As this work is based on our previous research [21], the mathematical model is similar to that conducted in Ref [21]. However, the simulation strategy for this work is slightly different due to the different system structures. Thus, the correctness of the system simulation program is still needed to

be verified. In order to conduct the simulation validation, we firstly take out a set of simulation results based on the initial working condition given in Table 1. The details of the simulation results are shown in Table 2. A series of verification items are selected to make the simulation validation on basis of these simulation results, shown as follows:

(1) Check whether $c_P m_{WS}(T_{16}-T_{15}) = A_{SC}\cdot I\cdot(\alpha\tau - k(T_{ave}-T_a)/I)$ is true;

(2) Check whether $U_G A_G \frac{(T_{16}-T_2)-(T_{17}-T_1)}{\ln((T_{16}-T_2)/(T_{17}-T_1))} = m_3 h_3 + m_2 h_2 - m_1 h_1$ is true;

(3) Check whether $U_{Ab} A_{Ab} \frac{(T_9-T_{18})-(T_{10}-T_{19})}{\ln((T_9-T_{18})/(T_{10}-T_{19}))} = m_9(h_9-h_{10})$ is true;

(4) Check whether $U_E A_E \Delta T_{lm,E} = m_5 h_5 + m_{14} h_{14} - m_{13} h_{13}$ is true;

(5) Check whether $m_2(h_2-h_7) = m_1(h_{11}-h_1)$ is true;

(6) Check whether the value of W_T/Q_E match the given value in the simulation.

The validation results show that all these items above match well, which indicates the simulation programs for this proposed cycle is rational. Further, a performance comparison between this cycle and other OTEC cycles are made in the following part.

Table 2

Results of simulation at the initial working condition (X_r=0.7 kg kg^{-1}, P_G=1.0MPa, m_3=1kg/s)

state	T (K)	p (MPa)	h (kJ kg^{-1})	m (kg/s)	X (kg kg^{-1})
1	310.56	1.00	-34.52	2.14	0.70
2	348.00	1.00	121.35	1.14	0.64

3	348.00	1.00	1610.06	1.00	0.99
4	316.20	0.67	1546.35	1.00	0.99
5	258.00	0.10	1456.11	0.24	0.99
6	291.54	0.37	1506.96	1.24	0.99
7	295.21	1.00	-182.63	1.14	0.43
8	293.22	0.38	696.32	2.37	0.72
9	291.75	0.38	587.55	2.64	0.70
10	282.00	0.38	-197.35	2.64	0.70
11	280.70	1.00	-196.36	2.14	0.70
12	282.00	0.38	-197.35	0.50	0.70
13	255.00	0.10	-197.35	0.50	0.70
14	258.00	0.10	-373.70	0.27	0.61
15	299.00	0.10	109.05	26	-
16	353.00	0.10	334.94	26	-
17	351.18	0.10	327.35	26	-
18	277.00	0.10	16.87	26	-
19	278.98	0.10	25.20	26	-

4.4. Results comparison

With a set of similar initial inputs, the performance of this combined cycle is compared to four OTEC power cycles: the absorption ejector OTEC cycle proposed by Yuan [21], the solar-assisted OTEC power cycle proposed by Yamada [9], the closed-cycle OTEC power cycle proposed by Aydin[8] and the experimental based closed-cycle OTEC power cycle proposed by Faizal [31]. Since

all of these four cycles are proposed for power generation purpose, in this section the power efficiency is considered as the key parameter which can reflect the performance of these cycles.

Table 3

Performance comparison of OTEC cycles under similar initial working conditions

	This study	Yuan [21]	Yamada [9]	Aydin [8]	Faizal [31]
Theoretical/Experimental research	Theoretical	Theoretical	Theoretical	Theoretical	Experimental
Cycle type	Solar-assisted combined cycle	Absorption ejector OTEC power cycle	Solar-assisted OTEC power cycle	Closed-cycle OTEC power cycle	Closed-cycle OTEC power cycle
Working fluid	Ammonia/water	Ammonia/water	Ammonia	R-32	R-134-a
Seawater inlet temperature (K)					
Warm seawater	299	299	298.7	299	300
Cold seawater	277	277	277.4	278	277.5-278
Component efficiency (%)					
Turbine	85	85	80	-	-
Solution pump	75	85	75	75	-
Seawater pump	80	85	80	80	-
Heat transfer coefficient (kW m^{-2} K^{-1})					

Generator	4.0	-	4.0	-	-
Absorber	3.5	-	3.5	-	-
Evaporator	4.0	-	-	-	-
Turbine/Pump work (kW)					
Turbine power work	170.73	71.17	100.1	100.0	-
Solution pump work	8.49	3.55	2.1	6.2	-
Warm seawater pump work	6.13	-	9.5	8.9	-
Cold seawater pump work	17.84	-	18.6	16.9	-
Refrigeration output (kW)	341.55	-	-	-	-
Power efficiency (%)	2.27	2.94	2.3	1.9	0.8-1.1
Effective efficiency (%)	7.89	-	-	-	-

As is shown in Table 3, the power efficiency of this proposed combined cycle is 2.27%, lower than that of 2.94% of the cycle in Ref. [21]. This is attributed to the following two main reasons: firstly, the solar collector efficiency is considered in the total power efficiency, which leads to a greatly decrease of the power efficiency; secondly, the turbine and pump efficiencies assumed in the latter cycle is at a higher value. Furthermore, the combined cycle in this study has a slightly lower power efficiency compared with the solar-assisted OTEC power cycle proposed by Yamada [9]. This is because in the combined cycle, an additional pump is introduced between the evaporator and the absorber, which consumes more energy. Besides, the heat absorbed in the evaporator eventually flows into the absorber, which leads to a higher energy consumption in the cold seawater pump. These factors all result in a slightly lower power efficiency of the combined cycle. Moreover, the closed-cycle OTEC power cycle showed the lowest theoretical power efficiency, due to a bigger heat transfer rate is required at the evaporator in the R-32 based cycle [8]. In addition, Faizal [31] conducted an

299 experimental research on the closed-cycle OTEC power cycle. With a similar heating and cooling
300 source temperature and the R-134-a as working fluid, the experimental power efficiency was obtained
301 at 0.8-1.1%. This practical power efficiency is at a relatively low level, due to that the turbine and
302 pump efficiencies and the evaporator/condenser heat transfer efficiencies are greatly limited in the
303 lab-scale experiment.

304 Besides of the power output, the refrigeration output is also produced in this combined cycle. It
305 is found the refrigeration output of the proposed cycle reaches to 341.55kW under the given condition.
306 Moreover, the contribution of refrigeration output on to is accessed by the effective efficiency (based
307 on Eq. (33)). Results in Table 3 shows that this combined cycle can reach to 7.89% under the initial
308 working condition, which greatly enhance the cycle performance.

309

310 The COP of this proposed cycle is compared with a solar-assisted double turbine combined cycle
311 that investigated by R. Shakar [32]. With a set of similar initial working conditions, the detailed results
312 are shown in Table 4.

313 **Table 4 COP comparison of combined cycles under similar initial working conditions**

	This study	R. Shakar [32]
Cycle type	Solar-assisted combined cycle	Solar-assisted combined cycle
Working fluid	Ammonia/ water	Ammonia
Solar collector outlet temperature (K)	393	393
Cooling source temperature (K)	277	303
Component efficiency (%)		

Turbine	85	75
Solution pump	75	75
Seawater pump	80	-
Heat transfer coefficient (kW m^{-2} K^{-1})		
Generator	4.0	-
Absorber	3.5	-
Evaporator	4.0	-
Refrigeration temperature at the evaporator inlet (K)	255	256
Turbine power work (kW)	192.8	11.5
Refrigeration output (kW)	386.3	18.5
Power efficiency (%)	2.35	1.93
COP	0.18	0.174

As is shown in Table 4, the combined power and refrigeration cycle in this study obtained slightly higher power efficiency and a slightly higher COP. These are reasonable results since the cooling source temperature of the cycle in this study is lower than the compared cycle in Ref. [32]. In this study, the cooling source is selected as the cold seawater; while the cooling source for the cycle in Ref. [32] is selected as the air.

Also, it is found that the COP of both of these combined cycles is at relatively low level. According to literatures [33, 34], with the heating source temperature at 393-423K and cooling source temperature below 273K, the COP of an individual single-effect ammonia/water absorption refrigeration cycle can reach to a much higher level of 0.5-0.7.

In summary, the following conclusions are obtained according to these comparison results:

• Compared with that of the individual OTEC power cycle, this combined power and refrigeration cycle has a slightly lower level of power efficiency;

• This combined power and refrigeration cycle has a high effective efficiency which weighted the produced refrigeration;

• Compared with that of the individual ammonia/water refrigeration cycle, this combined power and refrigeration cycle has a lower level of COP, but it is an energy generation system rather than an energy consumption system.

From the thermodynamic viewpoints, the individual OTEC power cycle utilizes the heated ammonia vapour to drive the turbine and produce power, and then the exhausted vapour is directly absorbed in the absorber. Compared with this process, the combined power and refrigeration cycle in this study also utilizes the heated ammonia vapour to produce power, so the turbine power output is produced under a similar condition. But in the combined cycle, an additional pump is introduced between the evaporator and the absorber, which consumes more energy. Besides, the heat absorbed in the evaporator eventually flows into the absorber, which leads to a higher energy consumption in the cold seawater pump. These factors all result in a slightly lower power efficiency of the combined cycle.

However, an additional process is introduced in this combined cycle: the exhausted vapour is used to drive the ejector that connected with the evaporator, thus the ammonia vapour generated from the evaporator is injected into the absorber and the evaporation process is enhanced. Therefore, this combined cycle has a slightly lower power efficiency compared with that of the individual OTEC power cycle, but it has a high effectively efficiency which weighted the produced refrigeration.

346 Moreover, in this combined power and refrigeration cycle the low grade energy is not totally
347 utilized to produce the refrigeration. In fact, large amount of the absorbed energy is converted to the
348 turbine power, which makes the COP of the combined power and refrigeration cycle at a lower level.
349 But unlike the individual ammonia/water refrigeration cycle which deems to be an energy
350 consumption system, the combined cycle is an energy generation system.

351 It is important to note that the refrigeration produced by this combined cycle is valuable for the
352 OTEC system. Unlike the individual OTEC power cycle, the combined power and refrigeration cycle
353 can produce both power and refrigeration based on the ocean thermal energy. Considering that a part
354 of turbine power work is consumed by the solution pumps and seawater pumps, the net power output
355 of the OTEC system is largely reduced. Nevertheless, according to the simulation results, in the
356 combined cycle the refrigeration can reach to approximately 2.48 times of the turbine power output,
357 which is very beneficial for the low-efficiency OTEC system.

358 Further, the performance comparison between the solar-assisted cycle in this study and the
359 absorption ejector OTEC cycle in Ref. [21] with the variation initial condition of generation pressure
360 and temperature is studied in this work. Fig. 3 shows that as the generation pressure varies, the power
361 efficiency of the proposed cycle remains at a lower range of 2.03%-2.31%, the power efficiency of
362 the compared OTEC cycle is at 2.67%-3.46%, and the effective efficiency of the proposed cycle can
363 reach to a higher level of 7.92%-7.64%. Moreover, it is found that the effective efficiency increases
364 to a peak value as the generation pressure increases. This behavior is caused by the following two
365 reasons: on one hand, Q_G decreases as P_G increases, so the effective efficiency increases since both W_T
366 and Q_E remain unchanged. On the other hand, solution concentration difference ΔX (X_r-X_w) decreases
367 as P_G increases (according to Eq. (20) and (21)). When ΔX approaches to zero, m_3 will decrease rapidly
368 and dominate the performance of the cycle, thus the effective efficiency decrease under this
369 circumstance. Fig. 4 shows that as the generation temperature increases, the power and effective

efficiency of both cycles climb up. The ranking of the efficiencies is similar to that obtained in Fig. 3. However, with the assistance of the flat-plate solar collector, the proposed cycle has a much wider generation temperature range.

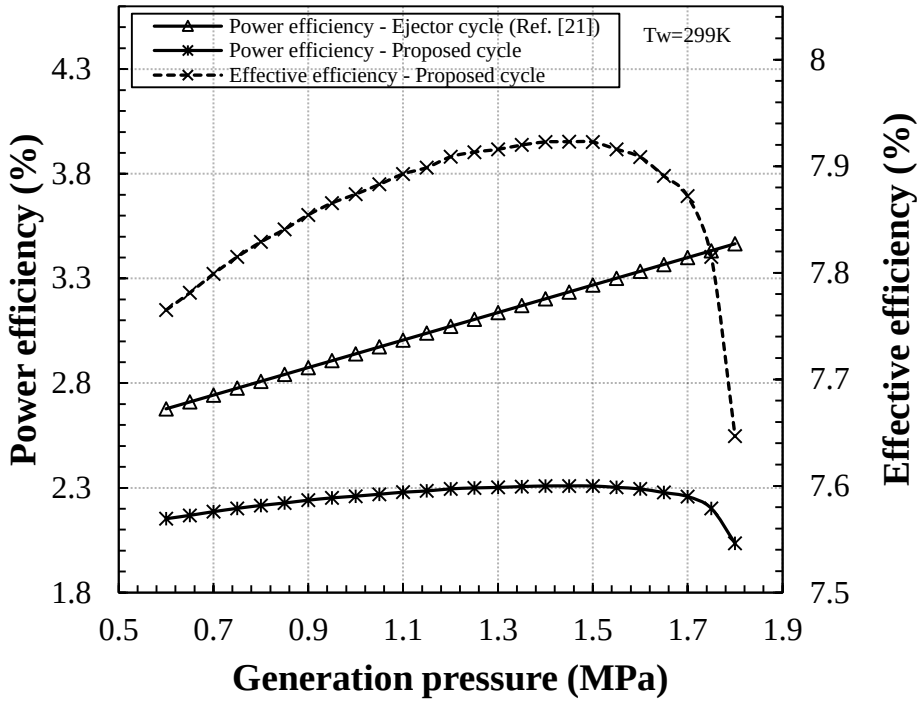

Fig. 3 Comparison between proposed cycle and OTEC cycle (Ref. [21] **) as P_G varies**

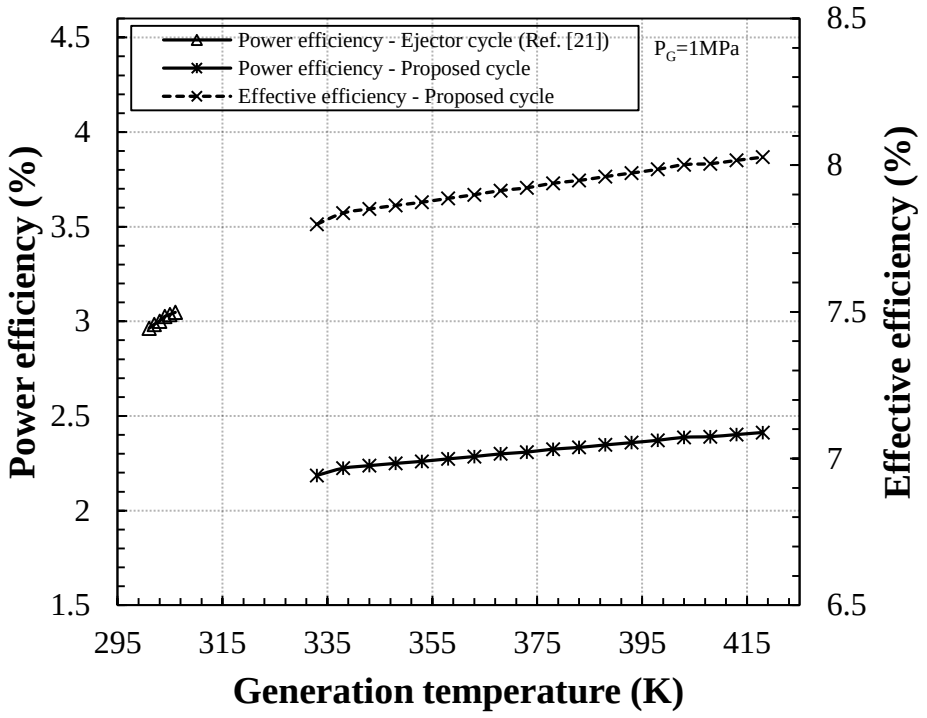

375

376 **Fig. 4 Comparison between proposed cycle and OTEC cycle (Ref.** [21]**) as T_G varies**

377

378 **5. Parametric analysis and discussions**

379 To further assess the effect of parameters on the performance of the proposed combined cycle, a
380 parametric analysis is conducted. And the simulation conditions are listed in Table 5.

381 **Table 5**

382 Conditions of simulation for the combined cycle

Generation temperature (K)	333-418
Generation pressure (MPa)	0.6-1.8
Strong solution concentration (kg kg^{-1})	0.55-0.9
Ammonia vapor mass flow rate (kg/s)	1
Power/refrigeration ratio	0.5

383 Based on the simulation conditions, the volumetric flow ratio (VFR) and size parameter (SP) of
384 turbine is investigated and the turbine isentropic efficiency can be obtained. According to Eq. (23)
385 and (24), the influences of generation temperature and pressure on turbine VFR and SP are
386 investigated and the results are shown in Fig. 5 and 6.

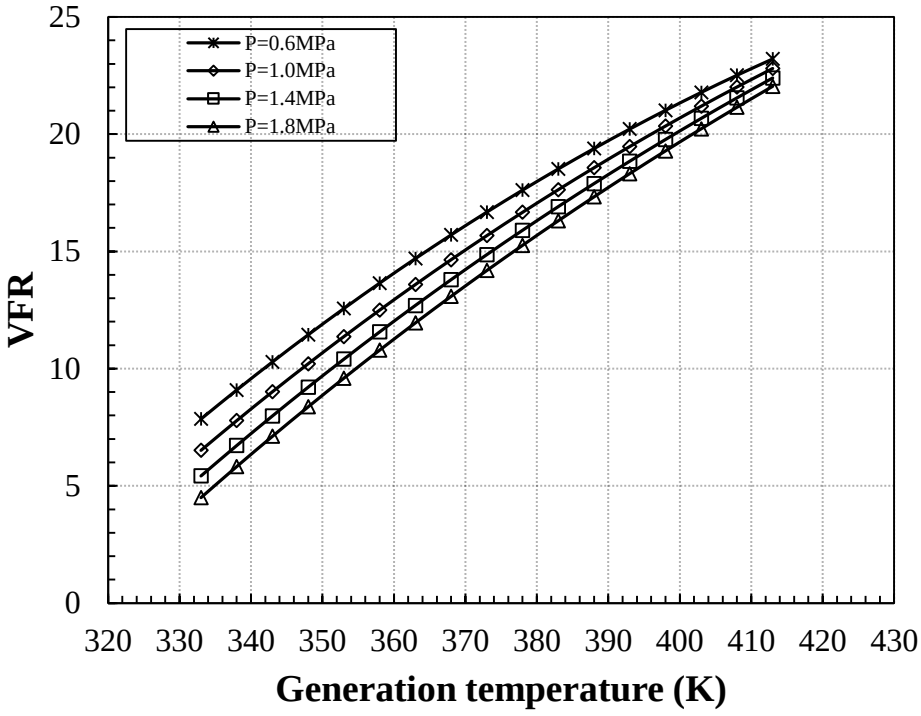

387
388 **Fig. 5 Volumetric flow ratio of turbine as T_G and P_G varies**

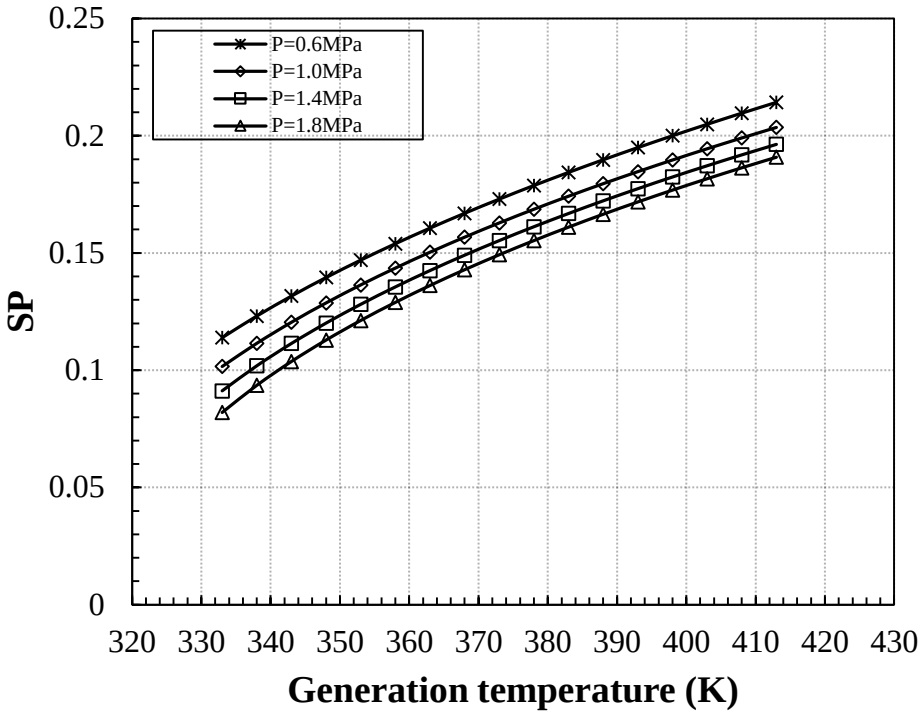

Fig. 6 Size parameter of turbine as T_G and P_G varies

It is found that higher generation temperature can lead to higher value of VFR and SP, while higher generation pressure leads to lower value of VFR and SP. Under the investigated operation condition of generation temperature at 333-418K and generation pressure at 0.6-1.8MPa, the VFR ranges in the value of 4.50-22.80 and the SP ranges in the value of 0.082-0.214. According to Ref. [35], the corresponding turbine efficiency can be obtained with these VFR and SP values. Thus in this study the turbine efficiency of the combined cycle is fixed at 85%.

5.1. Effect of the generation pressure

Fig. 7 shows the effect of generation pressure on heating input of the generator. It is found that given a fixed rich solution concentration the heat input decreases as the generation pressure increases. In the combined cycle the heat input exists in the generation process, and the following reason explains this behavior: since X_r is fixed, the increase of P_G can lead to a higher saturation temperature in

generator inlet, and thus h_1 increases (according to Sulze Equation); simultaneously, the increase of P_G also leads to an increase of m_1. So Q_G decreases (according to Eq. (19)). Furthermore, it is also found that higher rich solution concentration leads to a lower heat input. This is because h_1 is higher as X_r is fixed at a higher level, therefore Q_G decreases.

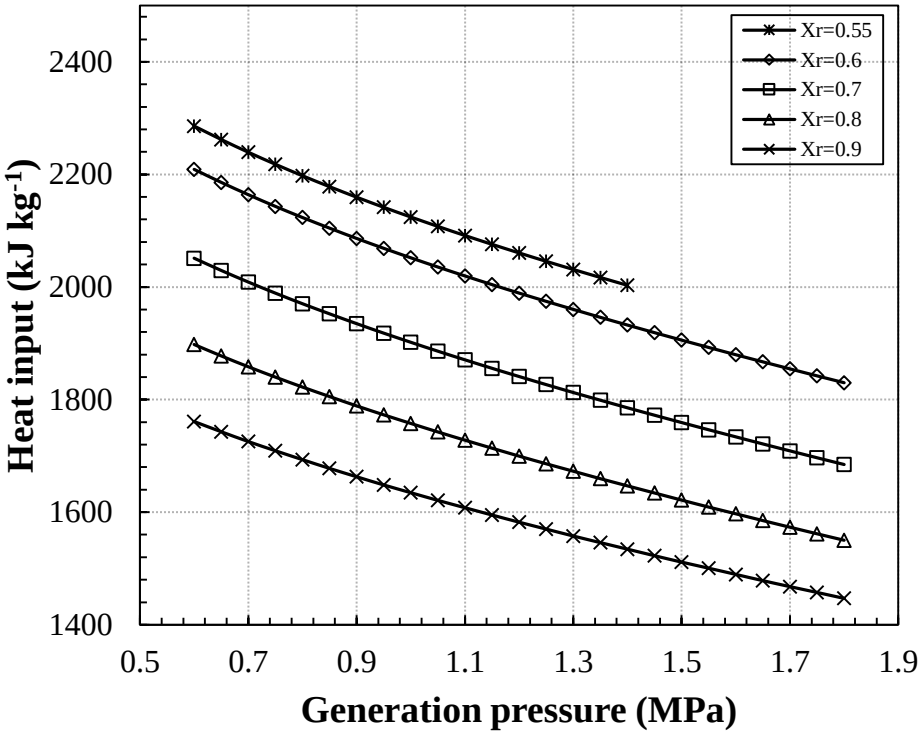

Fig. 7 Effect of generation pressure on heating input

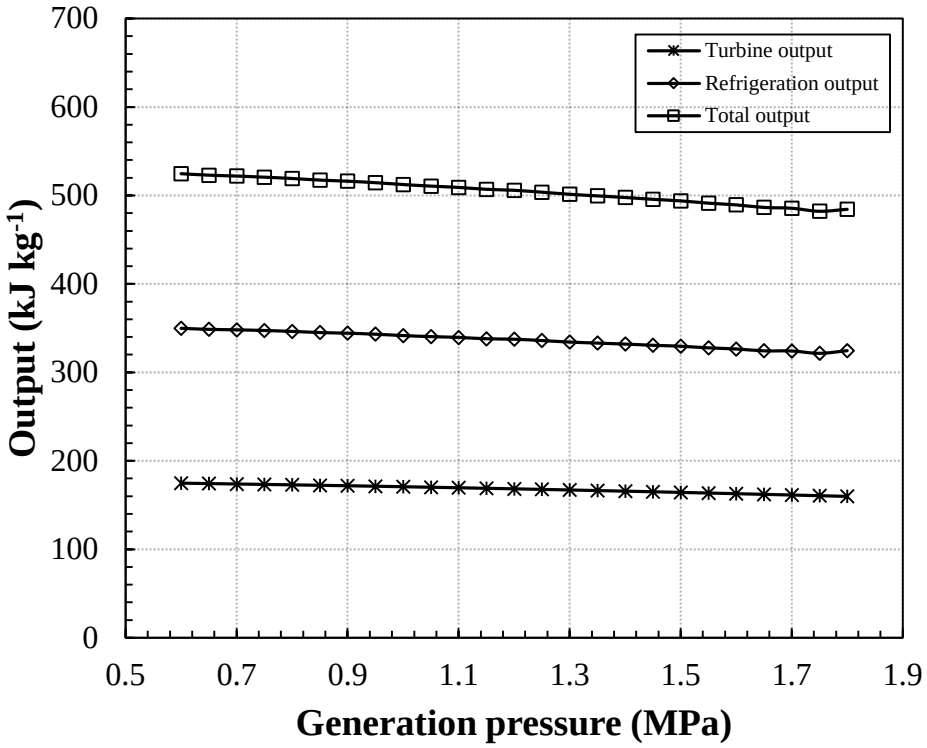

Fig. 8 Effect of generation pressure on output

Fig. 8 shows that the turbine outlet, refrigeration output and total output all see a slight decrease as the generation pressure varies. This behavior can be explained by noting that the turbine output W_T varies slightly as β remains the same, and the refrigeration output Q_E have the same trend for the power/refrigeration ratio is fixed.

Fig. 9 shows the effect of generation pressure on the effective efficiency. Firstly, it is found that the effective efficiency climbs up as the generation pressure increases, while it reaches to a peak value with a higher generation pressure and lower rich solution concentration. This behavior well matches that obtained in Fig. 7, and the explanation has been made above. It can also be found that higher X_r leads to a higher η. The reason is that Q_G decreases as X_r increases, and this ultimately leads to an decrease in heat input, so a higher η is obtained (according to Eq. (31)).

The entrainment ratio of the first-stage ejector (μ_I) is determined by m_4 and m_5, so it indicates the

relationship of the generation input and refrigeration output. The parametric analysis based on μ_I was also conducted and Fig. 10 shows the effect of generation pressure on entrainment ratio of ejector I. When X_r is higher (>0.7 kg kg^{-1}), it is found that the value of μ_I varies slightly as P_G increases. This is due to the following reason: as the power/refrigeration ratio is fixed and X_r in generator and evaporator is the same, m_4/m_5 will remain unchanged. Furthermore, it is also found that when X_r is lower, μ_I increases slightly as P_G increases, and then it see a rapid climb. The reason is that when P_G increases, X_w increases, thus ΔX decreases. When ΔX approaches to zero, the rapid decrease of m_3 ultimately leads to a rapid increase of μ_I.

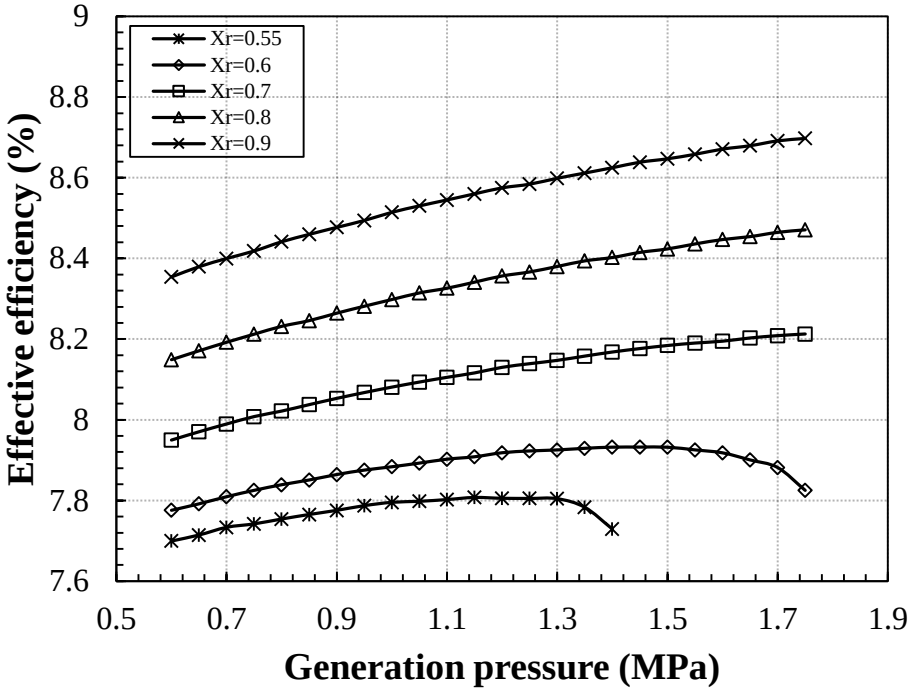

Fig. 9 Effect of generation pressure on effective efficiency

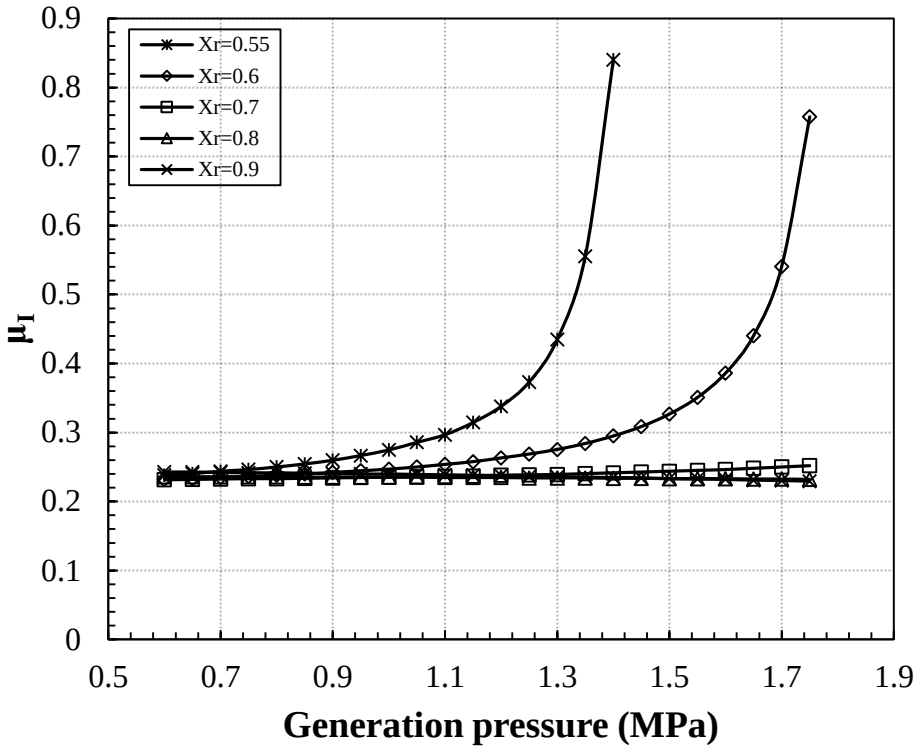

Fig. 10 Effect of generation pressure on entrainment ratio of ejector I

5.2. Effect of solar collector outlet temperature

In this cycle, the seawater is used as the heating source and the solar collector is introduced to rise the seawater temperature. The effect of solar collector outlet temperature on the cycle performance was accessed.

Fig. 11 shows that the heat input increases as the solar collector outlet temperature increases. This is due to the following reason: with a higher solar collector outlet temperature h_2 and h_3 is higher, while X_w is lower, which leads to a decrease in m_1 (according to Eq. (9) and (10)), thus the heat input get a higher value. It is also found that the heat input is lower with a higher X_r. This trend well matches the results obtained in Fig. 7.

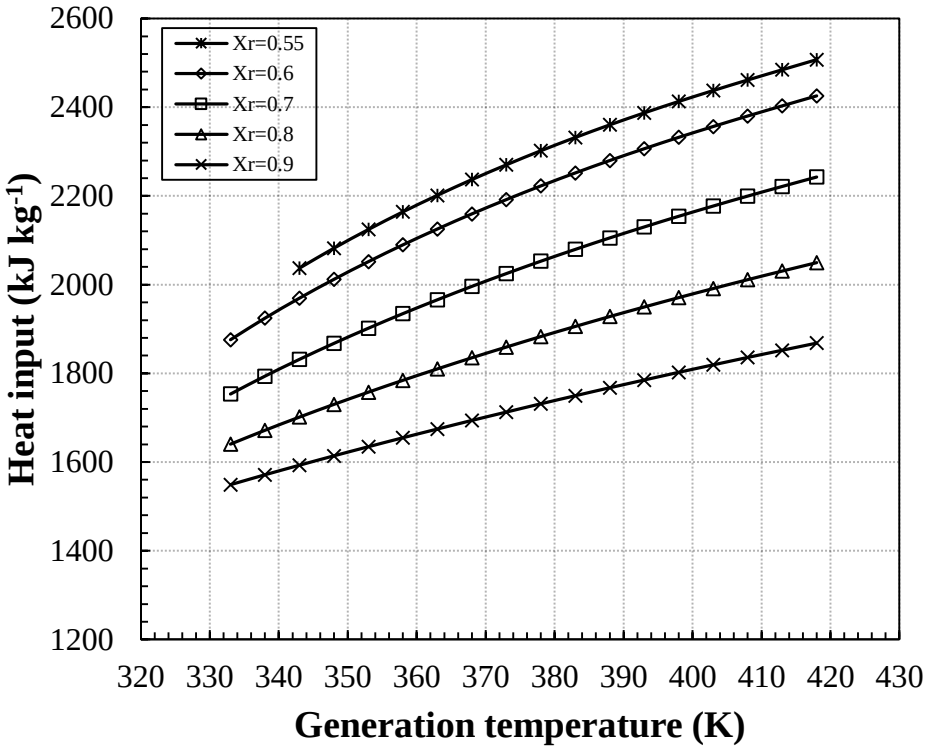

Fig. 11 Effect of solar collector outlet temperature on heating input

Fig. 12 reveals the relationship between solar collector outlet temperature and outputs of this cycle. Actually, a higher solar collector outlet temperature can be obtained by increasing either warm seawater pump flow rate or solar collector absorption area. It is found that increase of solar collector outlet temperature leads to higher outputs. This is because h_3 increases as the solar collector outlet temperature increases, so the turbine output increases with a fixed β. Besides, since the power/refrigeration ratio remains unchanged, the refrigeration output also increases. Thus the total output is higher. Further, Fig. 13 indicates that effective efficiency of this cycle can be enhanced by increasing solar collector outlet temperature. This behavior is caused by the combined effects of both heat input and cycle outputs.

Also, Fig. 13 shows that higher rich solution concentration leads to a higher effective efficiency, which has been obtained in Fig. 9.

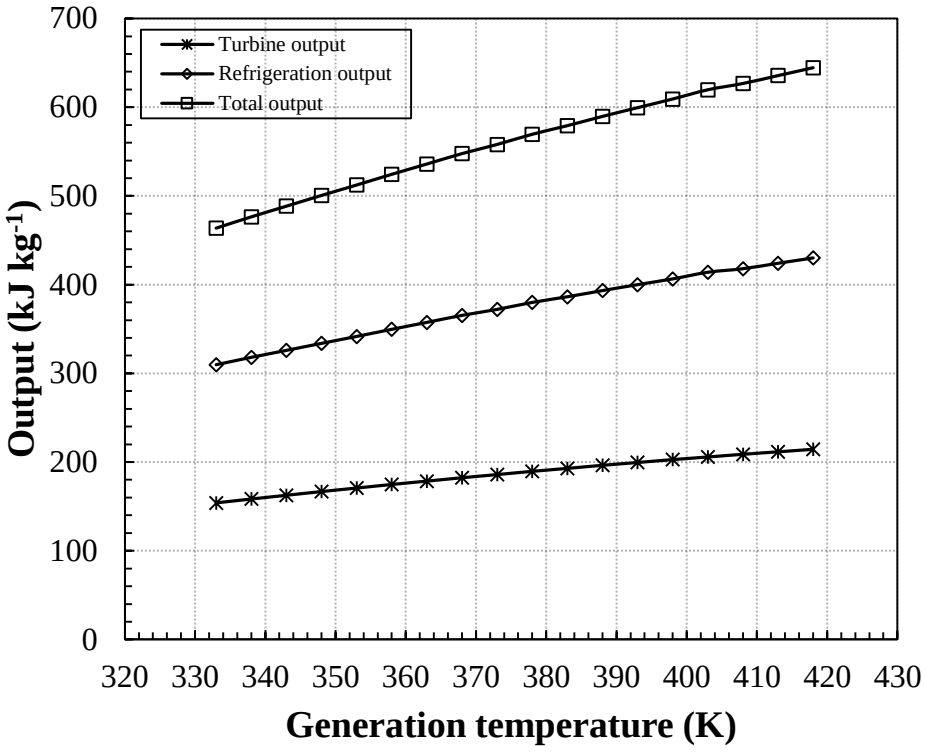

458

459 **Fig. 12 Effect of solar collector outlet temperature on output**

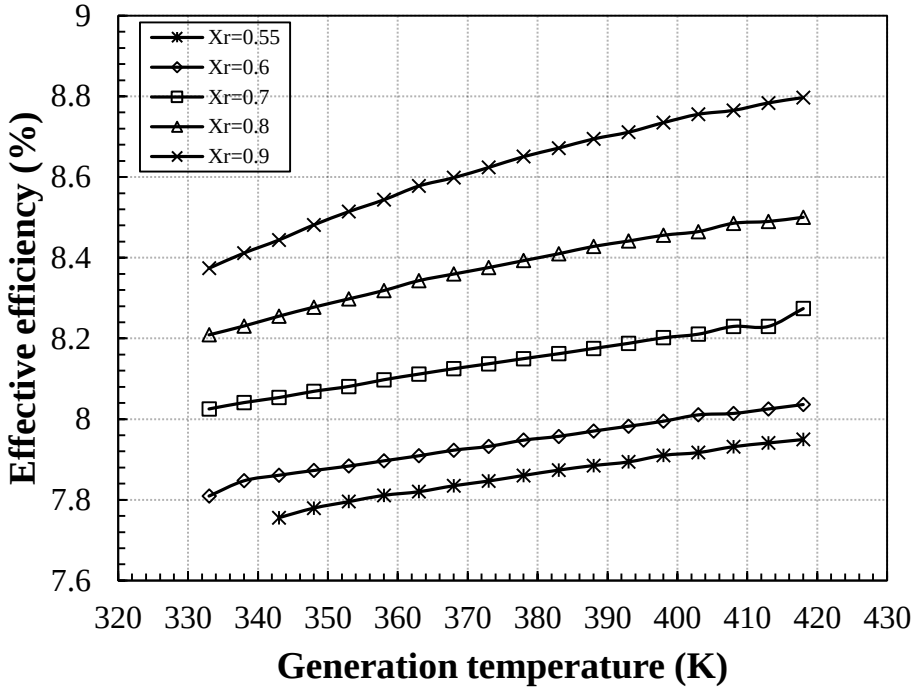

460

461 **Fig. 13 Effect of solar collector outlet temperature on effective efficiency**

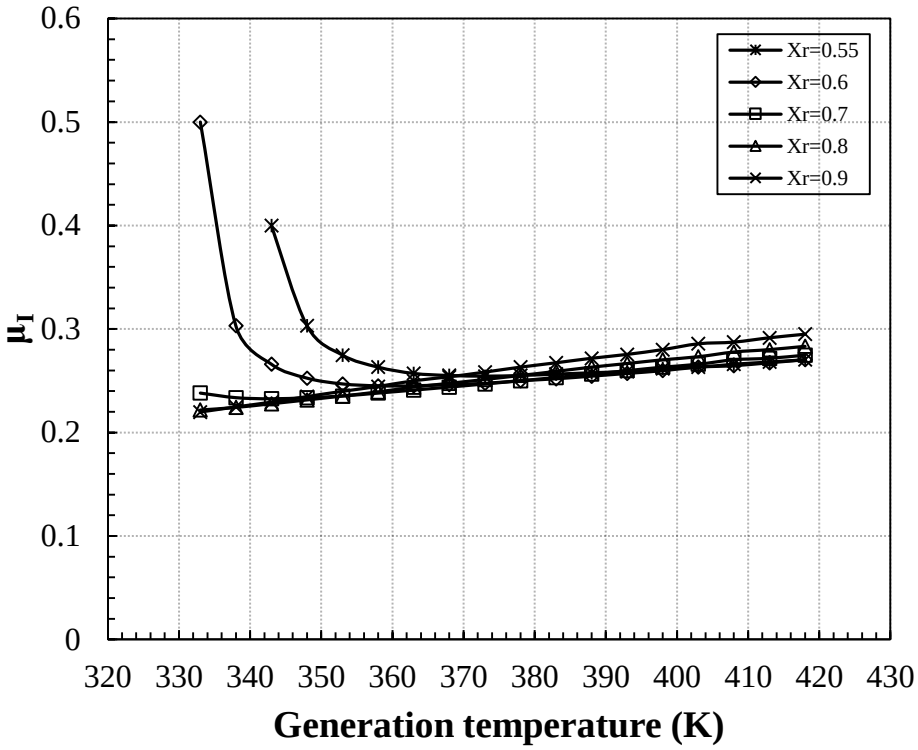

462

463 **Fig. 14 Effect of solar collector outlet temperature on entrainment ratio of ejector I**

464 Fig. 14 shows that the value of μ_I first drops rapidly with relatively lower solar collector outlet
465 temperature and rich solution concentration, and then it sees a steady increase as the solar collector
466 outlet temperature increases. The reason for the drop is as follows: when the solar collector outlet
467 temperature is lower, X_w is higher, thus ΔX is lower. When ΔX approaches to zero, m_4 will drop
468 rapidly, so μ_I will get a higher value (according to Eq. (13)).

469

470 **6. Conclusions**

471 This paper conducted a theoretical investigation on an OTEC based solar-assisted combined power
472 and refrigeration cycle. This combined can be utilized for both electricity and fishery cold storage
473 refrigeration generation. Mathematic model and simulation program for this proposed cycle were

developed; a performance comparison with previous studies was made; a parametric analysis was carried out to analyze the cycle performance. The main conclusions from this study can be summarized as follows:

• Compared with that of the individual OTEC power cycle, this combined power and refrigeration cycle has a slightly lower level of power efficiency.

• This combined power and refrigeration cycle has a high effective efficiency which weighted the produced refrigeration.

• Compared with that of the individual ammonia/water refrigeration cycle, this combined power and refrigeration cycle has a lower level of COP, but it is an energy generation system rather than an energy consumption system.

• Under the initial working condition, this combined cycle can reach to a power efficiency of 2.27% and effective efficiency of 7.89%. The refrigeration generation greatly enhances the cycle performance.

• The heat input, turbine output and refrigeration output decreases as the generation pressure increases, while it increases as the solar collector outlet temperature increases.

• The effective efficiency increases as the generation pressure increases, while it reaches to a peak value with a higher generation pressure and lower rich solution concentration.

• The effective efficiency increases as the solar collector outlet temperature increases.

• Higher rich solution concentration leads to a lower heat input but a higher effective efficiency.

• The entrainment ratio of the first-stage ejector is greatly affected by the rich solution concentration.

Acknowledgement

The authors acknowledge the support provided by the National Natural Science Foundation of China (NO. 51276174). H. Yuan is supported by the China Scholarship Council for a two-year research at University of Strathclyde.

References

[1] I.M. Putri, D.R. Munaf, Increasing Fishery Economic Added Value through Post Fishing Program: Cold Storage Program.
[2] F.A. McHale, W.L. Jones, H.M. Horn, Deployment and Operation of the 50KW Mini-OTEC Plant, in, Offshore Technology Conference.
[3] T. Mitsui, F. Ito, Y. Seya, Y. Nakamoto, Outline Of The 100 kw Otec Pilot Plant In The Republic Of Naure, Power Apparatus and Systems, IEEE Transactions on, (1983) 3167-3171.
[4] G. Nihous, M. Syed, L. Vega, Conceptual design of an open-cycle OTEC plant for the production of electricity and fresh water in a Pacific island, in: Ocean Energy Recovery, ASCE, 1990, pp. 207-216.
[5] P. Bombarda, C. Invernizzi, M. Gaia, Performance Analysis of OTEC Plants With Multilevel Organic Rankine Cycle and Solar Hybridization, Journal of Engineering for Gas Turbines and Power, 135 (2013) 042302-042302.
[6] R. Soto, J. Vergara, Thermal power plant efficiency enhancement with Ocean Thermal Energy Conversion, Applied Thermal Engineering, 62 (2014) 105-112.
[7] K. Rajagopalan, G.C. Nihous, Estimates of global Ocean Thermal Energy Conversion (OTEC) resources using an ocean general circulation model, Renewable Energy, 50 (2013) 532-540.
[8] H. Aydin, H.-S. Lee, H.-J. Kim, S.K. Shin, K. Park, Off-design performance analysis of a closed-cycle ocean thermal energy conversion system with solar thermal preheating and superheating, Renewable Energy, 72 (2014) 154-163.
[9] Y. Noboru, H. Akira, I. Yasuyuki, Thermal Efficiency Enhancement of Ocean Thermal Energy Conversion (OTEC) Using Solar Thermal Energy, in: 4th International Energy Conversion Engineering Conference and Exhibit (IECEC), American Institute of Aeronautics and Astronautics, 2006.
[10] N. Yamada, A. Hoshi, Y. Ikegami, Performance simulation of solar-boosted ocean thermal energy conversion plant, Renewable Energy, 34 (2009) 1752-1758.
[11] F. Sun, Y. Ikegami, B. Jia, A study on Kalina solar system with an auxiliary superheater, Renewable Energy, 41 (2012) 210-219.
[12] F. Sun, Y. Ikegami, H. Arima, W. Zhou, Performance Analysis of the Low-Temperature Solar-Boosted Power Generation System—Part I: Comparison Between Kalina Solar System and Rankine Solar System, Journal of solar energy engineering, 135 (2013) 011006.
[13] H. Yuan, N. Mei, S. Hu, L. Wang, S. Yang, Experimental investigation on an ammonia-water based ocean thermal energy conversion system, Applied Thermal Engineering, 61 (2013) 327-333.
[14] H. Uehara, Y. Ikegami, Parametric performance analysis of OTEC using Kalina cycle, ASME, NEW YORK, NY(USA). (1993) 203-207.

[15] T. Morisaki, Y. Ikegami, Performance Evaluation of Heat Exchangers in OTEC Using Ammonia/Water Mixture as Working Fluid, Open Journal of Fluid Dynamics, 2013 (2013).
[16] P.K. Nag, A.V.S.S.K.S. Gupta, Exergy analysis of the Kalina cycle, Applied Thermal Engineering, 18 (1998) 427-439.
[17] H. Yuan, N. Mei, Y. Li, S. Yang, S. Hu, Y. Han, Theoretical and experimental investigation on a liquid-gas ejector power cycle using ammonia-water, Science China Technological Sciences, 56 (2013) 2289-2298.
[18] D. Meinel, C. Wieland, H. Spliethoff, Effect and comparison of different working fluids on a two-stage organic rankine cycle (ORC) concept, Applied Thermal Engineering, 63 (2014) 246-253.
[19] A.I. Kalina, Combined-cycle system with novel bottoming cycle, Journal of Engineering for Gas Turbines and Power, 106 (1984) 737-742.
[20] H. Uehara, Y. Ikegami, Optimization of a Closed-Cycle OTEC System, Journal of solar energy engineering, 112 (1990) 247-256.
[21] H. Yuan, N. Mei, P. Zhou, Performance analysis of an absorption power cycle for ocean thermal energy conversion, Energy Conversion and Management, 87 (2014) 199-207.
[22] L.W. Florschuetz, Extension of the Hottel-Whillier model to the analysis of combined photovoltaic/thermal flat plate collectors, Solar Energy, 22 (1979) 361-366.
[23] J.H.N.E.P.L.F. Keenan, An investigation of ejector design by analysis and experiment, Massachusetts Institute of Technology, Guided Missiles Program, Cambridge, Mass., 1948.
[24] B.J. Huang, J.M. Chang, C.P. Wang, V.A. Petrenko, A 1-D analysis of ejector performance, International Journal of Refrigeration, 22 (1999) 354-364.
[25] Y. Dai, J. Wang, L. Gao, Exergy analysis, parametric analysis and optimization for a novel combined power and ejector refrigeration cycle, Applied Thermal Engineering, 29 (2009) 1983-1990.
[26] X.G. Li, Q.L. Zhang, X.J. Li, A Kalina cycle with ejector, Energy, 54 (2013) 212-219.
[27] G. Shu, X. Li, H. Tian, X. Liang, H. Wei, X. Wang, Alkanes as working fluids for high-temperature exhaust heat recovery of diesel engine using organic Rankine cycle, Applied Energy, 119 (2014) 204-217.
[28] H. Yuan, N. Mei, Energy, exergy analysis and working fluid selection of a Rankine cycle for subsea power system, Energy Conversion and Management, 101 (2015) 216-228.
[29] S. Vijayaraghavan, D.Y. Goswami, On Evaluating Efficiency of a Combined Power and Cooling Cycle, Journal of Energy Resources Technology, 125 (2003) 221-227.
[30] B. Ziegler, C. Trepp, Equation of state for ammonia-water mixtures, International Journal of Refrigeration, 7 (1984) 101-106.
[31] M. Faizal, M.R. Ahmed, Experimental studies on a closed cycle demonstration OTEC plant working on small temperature difference, Renewable Energy, 51 (2013) 234-240.
[32] R. Shankar, T. Srinivas, Parametric Optimization of Vapor Power and Cooling Cycle, Energy Procedia, 54 (2014) 135-141.
[33] S. Aphornratana, Theoretical and experimental investigation of a combined ejector-absorption refrigerator, in, University of Sheffield, Department of Mechanical and Process Engineering, 1995.
[34] P. Srikhirin, S. Aphornratana, S. Chungpaibulpatana, A review of absorption refrigeration technologies, Renewable and Sustainable Energy Reviews, 5 (2001) 343-372.
[35] E. Macchi, The choice of working fluid: the most important step for a successful organic Rankine cycle (and an efficient turbine), in: Second International Seminar on ORC Power Systems, Rotterdam, The Netherlands, Oct, 2013, pp. 7-8.

Figure captions

581

582 Table captions

Table 2 – Results of simulation at the initial working condition (X_r=0.7 kg kg^{-1}, P_G=1.0MPa, m_3=1kg/s)

Table 3 – Performance comparison of OTEC cycles under similar initial working conditions

Table 4 – COP comparison of combined cycles under similar initial working conditions

Table 5 – Conditions of simulation for the combined cycle

583